Prabha Materials Science Letters
Vol. 5, No. 1, 24-36, 2026
https://doi.org/10.33889/PMSL.2026.5.1.002

Theoretical Evaluation of Density and Radiation Shielding Performance of Fluoride Glasses

D. S. Kiran
Department of Physics,
Bangalore University, Bengaluru, Karnataka, India.
E-mail: kirands@bub.ernet.in

Susheela K. Lenkennavar
Department of Physics,
Bangalore University, Bengaluru, Karnataka, India.
Corresponding author: susheelakl@bub.ernet.in

(Received on August 26, 2025; Revised on October 2, 2025 & October 8, 2025 & October 13, 2025;
Accepted on October 29, 2025)

Abstract
This work investigated an empirical equation to predict the density of different fluoride glass compositions. The calculated values showed a close match with the theoretical density model proposed by Makishima and Mackenzie (1973), showed strong agreement with the experimental values. The calculations were used some compositional factors including molecular weight, molecular fractions, and the ionic radii of different elements mixed with fluoride, the values of ionic radii derived from "Revised Effective Ionic Radii and Systematic Studies of Interatomic Distances in Halides and Chalcogenides" (Shannon, 1976). In order to theoretically evaluate the radiation shielding properties of fluoride glasses, such as the Mean Free Path (MFP), Half-Value Layer (HVL), Tenth-Value Layer (TVL), Linear Attenuation Coefficient (LAC), and Mass Attenuation Coefficient (MAC), the density value is essential (Inaba and Fujino, 2010).

Keywords- Mass attenuation coefficient, Half-value layer, Mean free path, Molecular weight, Ionic radii.

1. Introduction

Glass is so prevalent in our daily surroundings that we often overlook its presence. In ancient Egypt, glass was regarded as a valuable material. Before that, prehistoric humans utilized sharp fragments of obsidian, a naturally occurring volcanic glass, to create tools and weapons such as scrapers, knives, axes, spears, and arrowheads. For thousands of years, humans have created glass by melting various raw materials, including sea salt (NaCl), bones (CaO), and sand (SiO_2). Naturally occurring glass, formed from the cooling of molten rock or lava, comprises a diverse range of components, such as alkali, alkaline earth metals, and transition metal oxides (Stroganova et al., 2003; Shelby, 2005; Le Bourhis, 2014). Initially, glass served solely as a decorative element. However, advancements in glass manufacturing techniques have significantly increased the material's value, leading to its essential role in various scientific applications across numerous technological domains. These include electronic devices, telecommunications (Ahmmad et al., 2021), optoelectronic systems, photonics (Boutarfaia et al., 2002; Nazabal et al., 2012), laser optics, biosensors (Panda et al., 2022), biomedicine, and radioactive waste storage, in addition to traditional uses such as windows, battery technology (El-Desoky et al., 2021; Abdel-karim et al., 2023), lenses, architecture and containers (Donald et al., 1997; Brauer et al., 2011; Musgraves et al., 2011). Physical properties of the glass, such as density, optical properties (Shaukat et al., 2001; Alsaif et al., 2023), thermal properties, chemical properties, mechanical properties (Mishra et al., 2024), brittleness, and viscosity, are directly linked to its versatility, and they define its broad range of industrial, scientific, and everyday applications (Doremus et al., 1974; Boolchand, 2000; Abd El-Moneim, 2019; Kawamoto et al., 2001).

Density is one of the fundamental properties of glass materials (Slater and Fong, 1982; Feller, 2015). It is defined as mass per unit volume and is commonly determined through Archimedes' principle by comparing the weight of glass in air and liquid (Macrelli et al., 2019). Density facilitates the calculation of various other attributes, including refractive index, strength-to-weight ratio, thermal conductivity, acoustic properties, elastic traits, and radiation shielding properties. From an academic perspective, density is associated with molar volume and ionic packing ratio. It is crucial to understand the structure of materials, whether inorganic, polymeric, or metallic (Inaba and Fujino, 2010). For glass, density is primarily influenced by its chemical composition. Therefore, the calculation of the density of the glass needs much attention from experts. Priven and Mazurin (2003) conducted a comparison of different methods for density estimation, revealing estimation errors ranging from 0.038 to 0.11 g/cm^3 for glasses with 450 mole% silica content (Scholze, 1991). It also provided a summary of several significant density models. In such a way, few studies were done on the oxide glasses to calculate density. However, no one worked on the fluoride glasses regarding the theoretical calculation of density.

Motivated by past research on oxide glasses, we adapted our approach to fluoride-based systems to evaluate their potential as radiation shielding materials. For this purpose, we referenced experimental density values from the literature to support the theoretical framework. In this investigation, we evaluated the packing density parameter and theoretical density of fluoride glasses, which revealed an excellent alignment with experimental values, confirming the validity of the applied model. Among the systems analyzed, the composition of IBSCZ fluoride glass showed a notably close alignment between theoretical and experimental density. Therefore, the Phy-X computational tool was used to assess this glass's radiation shielding properties, and the results were compared with conventional shielding materials.

2. Theoretical Procedure

2.1 Density Model

Using the theoretical density model of oxide glasses (Makishima and Mackenzie, 1973), we have calculated packing density parameters for coordination numbers 4 and 6 of fluoride compositions using ionic radii (Shannon and Prewitt, 1969; Shannon and Prewitt, 1970) and also calculated the density for the different fluoride glasses, Considering this model (Inaba and Fujino, 2010).

The empirical equation for the density determination of oxide glasses is

$$Vp = \rho \frac{\sum(V_i \cdot X_i)}{\sum(M_i \cdot X_i)} \quad (1)$$

$$\rho = Vp \frac{\sum(M_i \cdot X_i)}{\sum(V_i \cdot X_i)} \quad (2)$$

$$\rho = 0.53 \frac{\sum(M_i \cdot X_i)}{\sum(V_i \cdot X_i)} \quad (3)$$

where, they are treated as V_p ionic packing ratio, which is constant equal to 0.53, M_i is molar weight (g/mol), X_i is molar fraction (mol %), ρ is density (g/cm^3), and. V_i is the packing density parameter (m^3/ mol) obtained from the following equation for an oxide M_XO_Y. X denotes the number of metal atoms, and Y indicates the number of oxygen atoms in the compound M_XO_Y. For instance, in the case of GeO_2, X is equal to 1 and Y is equal to 2.

$$V_i = \frac{4}{3}\pi N_A(X\, r^3_M + Y\, r^3_O) \quad (4)$$

where, N_A is Avogadro's number (mol^{-1}) and r_M and r_O are the ionic radius of the metal and the ionic radius of the oxygen, respectively. In this study, ionic radii were used (Shannon, 1976). In the packing density

parameter equation, when we replace fluorine instead of oxygen, the composition will become $M_xF_{y.}$ X denotes the number of metal atoms, and Y indicates the number of fluorine atoms in the compound M_XF_Y. For instance, in the case of GeF_2, X is equal to 1 and Y is equal to 2. Then Equation (4) becomes as follows,

$$V_i=\frac{4}{3}\pi N_A(X\ r^3_M + Y\ r^3_F) \quad (5)$$

where. r_F is the ionic radius of the fluorine. By using these equations, we have calculated the packing density parameter and the density of the fluoride glass compositions.

2.2 Radiation Shielding Properties

The process of reducing ionizing radiation, like X-rays and gamma rays, by interposing materials in their path to reduce radiation intensity through scattering or absorption is referred to as radiation shielding. Thickness, density, and atomic composition these are all affect a material's capacity to attenuate incoming photons, which is a critical component of radiation shielding performance. The attenuation of photon beams as they traverse a shielding material follows the Beer–Lambert law, mathematically expressed as (Mariyappan et al., 2018; Gayathri et al., 2024; Ornketphon et al., 2024).

$$I = I_0 e^{-\mu x} \quad (6)$$

where, I_0 and I are the incident and transmitted photon intensities, respectively, μ is the linear attenuation coefficient (LAC), and x is the thickness of the material. This exponential relationship highlights that a higher LAC value indicates a material's superior ability to absorb or scatter photons, thereby enhancing its shielding effectiveness. To account for material density and allow comparison between different materials or compositions, the mass attenuation coefficient (MAC) is used. It normalizes the LAC by the material's density (ρ), and is given by

$$MAC = \frac{\mu}{\rho} \quad (7)$$

In practical uses of shielding analysis, the Linear Attenuation Coefficient (LAC) gives rise to a number of important parameters, such as the Half-Value Layer (HVL), Tenth-Value Layer (TVL), and Mean Free Path (MFP). The HVL is the thickness that will cut the amount of radiation in half. It directly shows how well a material protects against radiation. A smaller HVL means that the material is better at protecting against radiation. The TVL, on the other hand, is the thickness needed to decrease radiation levels to 10% of their original level. This is particularly crucial when designing safe places such as radiotherapy rooms and nuclear plants. Lastly, the Mean Free Path signifies the average distance a photon travels within the material before it interacts through absorption or scattering, with the relationships defined as

$$HVL = \frac{\ln 2}{\mu} = \frac{0.693}{\mu} \quad (8)$$

$$TVL = \frac{\ln 10}{\mu} = \frac{2.302}{\mu} \quad (9)$$

$$MFP = \frac{1}{\mu} \quad (10)$$

The Phy-X computational tool was used to theoretically evaluate the radiation shielding properties of the IBSCZ glass. This tool can calculate the above parameters for a wide range of photon energies. These kinds of studies are very important for figure out the glass systems in radiation shielding, especially in medical, nuclear and industrial settings, where, both protection and transparency are needed.

3. Result and Discussions

3.1 Density Model

The packing density parameter and density of the fluoride glass compositions are investigated in this work by utilizing Equations (5) and (3), respectively. **Table 1** shows the packing density parameter (V_i) for different fluoride chemical compositions for both 4 and 6 coordination numbers. Calculated V_i values are distinguished by small fractions, and not all elements have ionic radii for coordination number 4, but all elements have ionic radii for coordination number 6, and a coordination number of six was adopted, as the majority of fluoride glass constituents exhibit octahedral coordination in both crystalline analogues and glassy states. This selection ensures consistency with experimentally observed densities, reflects the inherent structural compactness of fluoride-based networks, and aligns with established structural models reported in the literature (Tanabe et al., 1995; Inaba and Fujino, 2010). So that while calculating the density of the different fluoride glass compositions, we have used the packing density value of coordination number 6. Equation (4) is satisfied for oxide glass compositions, and Equation (5) is satisfied for fluoride glass compositions. As we noted from the literature survey, there have been a lot of theoretical and empirical studies in the past for oxide glasses (Inaba and Fujino, 2010; Komatsu et al., 2021; Coskun et al., 2023; Kumar et al., 2024; Tian et al., 2024). Although fluoride glasses have been widely investigated experimentally, their theoretical modeling has not been explored to the same extent as oxide glasses. To bridge this gap, we have performed theoretical calculations for fluoride glasses using adapted models from oxide glass systems and compared them with experimental data, demonstrating that such calculations can be successfully extended to fluoride glasses.

Fluoride glass compositions, theoretical density values, and experimental density values are listed in **Table 2**. Experimental density values for the mentioned fluoride glass compositions were taken from the existing literature (Poulain et al., 1992), which was measured by using Archimedes' principle. Experimental values are closely matched with the theoretical density values obtained from the Equation (3). The relative error is roughly 0–8%, as indicated by the absolute deviations ($|\rho theo - \rho exp|$), which vary from 0.00 to 0.35 g/cm³. Since these deviations are affected by composition and do not follow a consistent trend, Equation (3) is considered a reliable method for estimating the densities of fluoride glasses without the need for a universal correction factor.

A histogram was plotted for the theoretical density values for the studied fluoride glass compositions as shown in **Figure 1**, which vary from 3.16 to 6.08 g/cm^3. The peaks indicate that the distribution of density values is around 3.0, 4.0-4.2, 5.0-5.3, and 6.08 g/cm^3. This reflects the effect of chemical compositions on the density values. The density values of glasses containing heavier cations, such as Th^{4+}, In^{3+}, Zn^{2+}, and Yb^{3+}, are higher than those of glasses containing lighter cations, such as Al^{3+}, Li^{+}, Na^{+}, and Mg^{2+}. With a deviation of 0-8%, **Table 2** demonstrates that theoretical values and experimental density values are in the good agreement. Among the fluoride glass compositions IBSCZ glass is exactly matched with the experimental value (5.10 g/cm^3), which confirms the reliability of the adopted density model. Density is a crucial parameter for governing the radiation shielding, optical, elastic properties (Shi et al., 2020) and physical properties of the fluoride glasses.

Density directly impacts the refractive index; the higher the density of a glass, the tighter its atomic packing, so when light passes through, it slows down and can be bent more. Density also correlates with dispersion; i.e., the splitting of light into a spectrum, which is a sought-after characteristic in devices for spreading light, such as lenses and prisms. As the density and refractive index of the glass increase reflectance also increases, while density does not solely dictate transparency, it indirectly affects light absorption, especially at higher wavelengths. Therefore, the density is crucial to determine such optical parameters as refractive

index, dispersion, and reflectance that underpin the development of glass designed for optical use (Halimah et al., 2018; Abouhaswa and Taha, 2024).

Table 1. Chemical Composition, Molecular weight (M_i), and Packing Density Parameter (V_i) for the coordination number 4 and coordination number 6 of the elements of the chemical composition.

Composition	Molar weight (M_i) (g/mol)	Packing density parameter (V_i) (10^{-6} m^3/mol), Coordination number 4	Packing density parameter (V_i) (10^{-6} m^3/mol), Coordination number 6
ZrF_4	167.22	23.19	24.671
BaF_2	175.32	-	18.069
LaF_3	195.9	-	20.801
ThF_4	308.03	-	26.046
AlF_3	83.98	17.15	18.184
NaF	41.99	8.115	8.6084
HfF_4	254.48	23.16	24.632
YF_3	145.9	-	19.636
CaF_2	78.08	-	14.312
ScF_3	101.96	-	18.84
CdF_2	150.41	12.534	14.166
ZnF_2	103.39	11.88	12.887
SrF_2	125.62	-	15.408
YbF_3	230.04	-	19.39
InF_3	171.81	17.60	19.088
MgF_2	62.3	11.80	12.806

Table 2. Glass composition, Theoretical density [ρ (g/m^3)], Experimental density [ρ (g/m^3)], Absolute deviation [Δρ (g/m^3)], and Relative error (%).

Glass code	Glass composition	Theoretical density ρ_{the} (g/cm^3)	Experimental density ρ_{exp} (g/cm^3)	Absolute deviation Δρ (g/cm^3)	Relative error (%)
ZBL	$62ZrF_4$-$33BaF_2$-$5LaF_3$	4.90	4.60	0.30	6.12
ZTL	$60ZrF_4$-$30ThF_4$-$10LaF_3$	5.32	5.25	0.07	1.31
ZBLA	$57ZrF_4$-$34BaF_2$-$5LaF_3$-$4AlF_3$	4.21	4.54	0.33	7.84
ZBLAN	53 ZrF_4-$20BaF_2$-$4LaF_3$-$3AlF_3$-20NaF	4.19	4.35	0.16	3.82
AYTB	$28.7AlF_3$-$28.7YF_3$-$22.6ThF_4$-$20BaF_2$	5.34	5.10	0.24	4.50
YABC	$20YF_3$-$40AlF_3$-$20BaF_2$-$20CaF_2$	4.12	4.00	0.12	2.91
TLB	$30ThF_4$-60LiF-$10BaF_2$	5.61	5.29	0.32	5.70
ZBTY	$28.3ZnF_2$-$15BaF_2$-$28.3ThF_4$-$28.3YbF_3$	6.08	6.43	0.35	5.76
IBSCZ	$40InF_3$-$15BaF_2$-$20SrF_2$-$5CdF_2$-$20ZnF_2$	5.10	5.10	0.00	0.00
ASCM	$39AlF_3$-$23SrF_2$-$28CaF_2$-$10MgF_2$	3.16	3.42	0.26	8.23

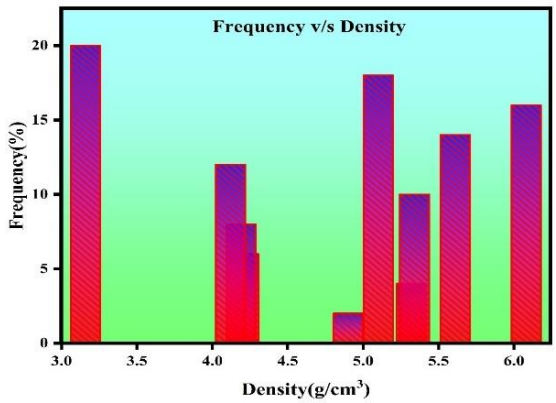

Figure 1. Theoretical density histogram of fluoride glass composition.

3.2 Radiation Shielding Properties

In many fields like industries, nuclear power plants, aerospace engineering, and medical imaging, where ionizing radiation exposure must be kept to a minimum, radiation shielding is essential. Despite their widespread use of traditional shielding materials like regular concrete, ilmenite, and hematite-serpentine frequently have drawbacks like limited flexibility and possible toxicity. Radiation shielding parameters, including MAC, LAC, HVL, TVL, and MFP values of conventional shielding materials, as well as density (**Table 3**) were gathered from publications already in existence (Bashter, 1997). Advanced materials that are not only more effective but also lightweight, transparent, and non-toxic are becoming more and more necessary as a result, because of their superior attenuation capabilities and advantageous physical characteristics. Fluoride-based heavy metal glasses, particularly those made of high atomic number (high-Z) elements have emerged as promising substitutes. We looked more closely at the radiation shielding qualities of IBSCZ glass because, in this case, it has a theoretical density value that is much more accurate than the experimental density value among the evaluated fluoride glasses. gamma-ray shielding properties of IBSCZ glass with the composition $40InF_3–15BaF_2–20SrF_2–5CdF_2–20ZnF_2$ has been evaluated. The fluorine-rich matrix improves the optical clarity and lower material weight, while the presence of In and Cd greatly improves photon interaction. Using crucial parameters like MFP, HVL, TVL, MAC, and LAC. This study methodically examines the shielding effectiveness of IBSCZ glass over a broad photon energy range (0.015–15 MeV). When the outcomes are contrasted with traditional shielding materials, it is evident that IBSCZ performs better. According to these results, IBSCZ glass is a cutting-edge radiation shielding substance that is perfect for portable and high-performing protective systems.

Table 3. Density (in g/cm^3) of shielding materials.

Shielding materials	Density in (g/cm^3)
Ordinary concrete	2.30
Hematite-Serpentine	2.50
Ilmenite-Limonite	2.90
Basalt-Magnetite	3.05
Ilmenite	3.50
IBSCZ glass	5.10

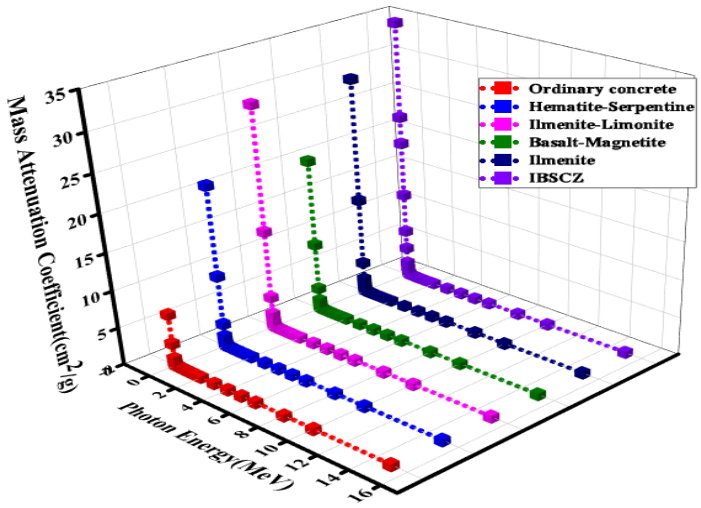

Figure 2. Mass attenuation coefficient of IBSCZ glass and other shielding materials.

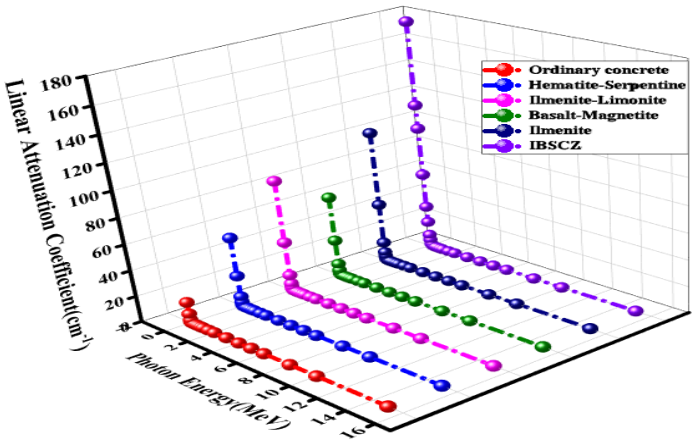

Figure 3. Linear attenuation coefficient of IBSCZ glass and other shielding materials.

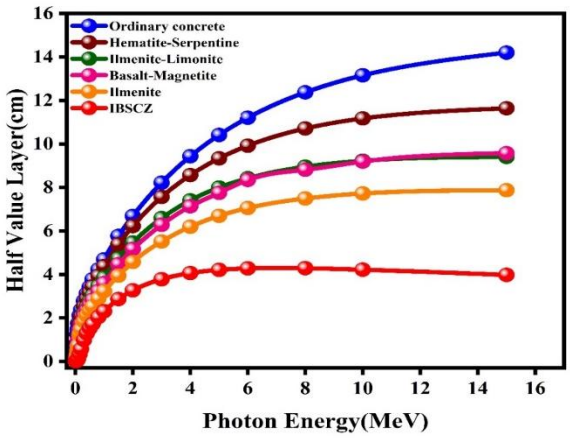

Figure 4. Half value layer of IBSCZ glass and other shielding materials.

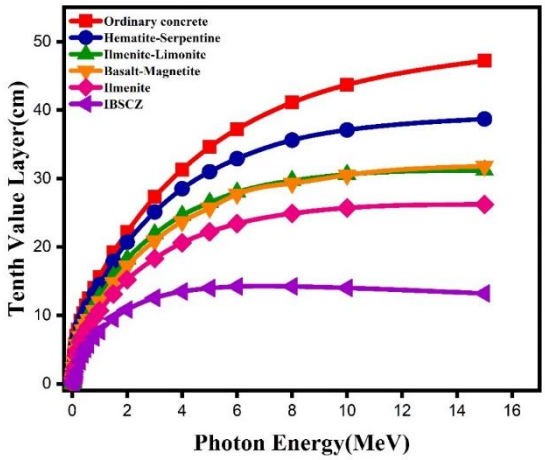

Figure 5. Tenth value layer of IBSCZ glass and other concrete materials.

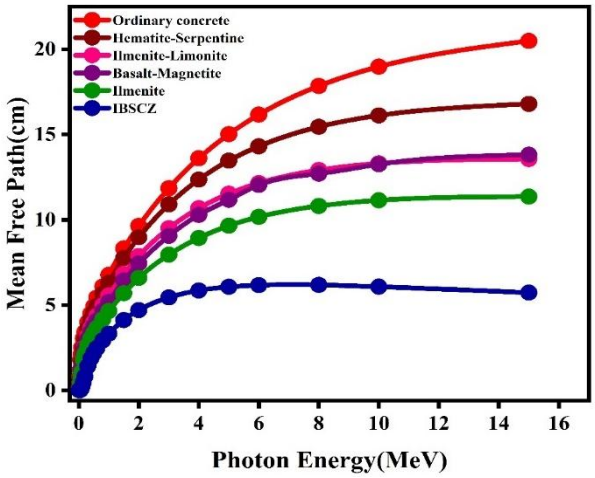

Figure 6. Mean free path of IBSCZ glass and other shielding materials.

IBSCZ shows the top MAC value of 34.53 cm^2/g at 0.015 MeV. This beats other materials like Ilmenite–limonite (29.64 cm^2/g) and Ilmenite (29.12 cm^2/g) by a wide margin. As photon energy rises, MAC values drop for every material. The reason is a shift from photoelectric absorption to Compton scattering. Still, IBSCZ keeps the lead in all cases (**Figure 2**). At 1 MeV and 10 MeV, IBSCZ reaches 0.059 cm^2/g and 0.032 cm^2/g which are still higher than the conventional shielding materials, which range from 0.021 to 0.034 cm^2/g respectively (Sekaran et al., 2024).

At 0.015 MeV energy level, IBSCZ has a high LAC value of 176.13 cm^{-1} as shown in **Figure 3**. This value is significantly higher than ilmenite (102.0 cm^{-1}), ilmenite–limonite (86.00 cm^{-1}), and ordinary concrete (16.28 cm^{-1}). It continuously maintains the highest values throughout entire energy range, while the LAC values for all materials reduces as the energy increases and Compton scattering takes over as the primary interaction mechanism. Other materials exhibit a LAC of 0.148 to 0.215 cm^{-1} at 1 MeV, whereas IBSCZ exhibits a LAC of 0.300 cm^{-1}. At extremely high energies, such as 15 MeV, where attenuation is more difficult, IBSCZ maintains a leading value of 0.174 cm^{-1} (Kumar et al., 2025a).

IBSCZ has a remarkably low HVL of only 0.004 cm at low photon energy (0.015 MeV), which is much lower than that of ilmenite (0.007 cm), ilmenite–limonite (0.008 cm), and ordinary concrete (0.043 cm). IBSCZ continuously maintains the lowest HVL throughout the spectrum as photon energy rises (**Figure 4**), indicating its high attenuation capacity. IBSCZ has an HVL of 2.307 cm at 1 MeV, whereas the HVL of other materials is between about 3.226 and more than 4.692 cm. IBSCZ exhibits HVLs of 4.215 cm and 3.974 cm, respectively, even at high energies like 10 MeV and 15 MeV, where shielding becomes more difficult. These values are significantly lower than those of conventional materials like concrete (13.15 and 14.19 cm) and ilmenite (7.722 and 7.872 cm) at the same order of energy (Mariyappan et al., 2018).

The TVL of the shielding materials is shown in **Figure 5**. IBSCZ exhibits an exceptionally low TVL of 0.013 cm at low photon energy (0.015 MeV), greatly surpassing concrete (0.141 cm), ilmenite (0.023 cm), and ilmenite–limonite (0.027 cm). All across the energy range, this exceptional performance is maintained. At 1 MeV Ilmenite and ordinary concrete have TVLs of 10.70 cm and 15.6 cm respectively, while IBSCZ records a TVL of 7.663 cm. IBSCZ maintains the lowest TVL of 13.20 cm even at high energies like 15

MeV, while ilmenite and concrete have TVLs of 26.20 cm and 47.2 cm, respectively (Kumar & Lenkennavar, 2025b).

The mean free path of shielding materials is shown in **Figure 6**. IBSCZ has a very low MFP of 0.006 cm at low photon energy (0.015 MeV), which is much lower than that of concrete (0.060 cm), ilmenite (0.010 cm), and ilmenite–limonite (0.012 cm). This suggests that IBSCZ is very effective for low-energy applications like diagnostic radiology because gamma photons are more likely to be absorbed or scattered within a shorter distance. Because the interaction probability decreases with increasing photon energy, MFP values increase for all materials; however, IBSCZ continuously maintains the lowest values throughout the spectrum. IBSCZ records an MFP of 3.328 cm at 1 MeV, whereas other materials have MFPs ranging from 4.655 to more than 6.770 cm. IBSCZ exhibits MFPs of 6.081 cm and 5.733 cm, respectively, even at high energies like 10 MeV and 15 MeV. These are significantly lower than those of concrete (18.979–20.488 cm) and ilmenite (11.143–11.360 cm) (Gayathri et al., 2024). However, the shielding efficiency of glass materials is naturally limited when photon energies surpass 10 MeV. Photonuclear reactions and pair production predominate in this regime, producing secondary neutrons and photons that reduce net attenuation. Therefore, even though IBSCZ performs better up to 15 MeV, it would need to be combined with neutron-absorbing additives or composite barrier systems to provide effective shielding at ultra-high energies (Judith and Oryema, 2024).

In comparison to other shielding materials, IBSCZ glass is a very effective and sophisticated material for gamma-ray shielding, as shown by the thorough examination of the radiation shielding parameters, including MAC, LAC, HVL, TVL, and MFP. Its superior performance is largely due to its fluorine-based composition, which contributes to desirable properties like high density, optical transparency, and reduced toxicity, as well as the presence of high atomic number elements like indium and cadmium, which increase the probability of photon interactions. All of the results point to IBSCZ glass's superior attenuation ability with low HVL, TVL, and MFP values, demonstrating how well it protects against radiation while being small, light, and non-toxic. These characteristics make IBSCZ glass a promising and versatile material for cutting-edge applications in medical imaging, nuclear facilities, and aerospace radiation shielding systems.

The glass systems contain heavy metal oxides like PBO and Bi2O3, which provide excellent gamma ray shielding due to their high atomic number and high density; however, these are have some limitations in practical applications because of their toxicity. The recent works reported that these borate glasses show high densities with superior gamma ray attenuation (Aloraini et al., 2021; Almugrin et al., 2022). Tellurate glasses having intermediate densities and which balances the shielding performance and optical transparency (Putra et al., 2025). In contrast, silicate glasses are light weight but they provide poor shielding performance. However, IBSCZ glass is a safer alternative that offers a balance between radiation protection and optical functionality because of its moderate density, wide UV–mid-IR transparency, and non-toxicity (Majewski et al., 2018).

The efficiency of the gamma ray shielding in glasses is determined by the combined effects of elemental composition and density, rather than density alone. Both the energy and the elemental makeup of the photons affect their interactions; elements with high atomic numbers (Z) enhance Compton scattering at intermediate energies and photoelectric absorption at lower energies. The IBSCZ glass has elements with mid-to-high atomic numbers (In, Cd, Ba, and Zn) and shows strong gamma-ray attenuation across 0.015-15 MeV. Cadmium increases neutron-capture efficiency at higher energies. Compared to denser but potentially hazardous thorium-based glasses (ZBTY, TLB, AYTB), IBSCZ offers a safer and more effective shielding performance. Excellent structural compactness is indicated by the perfect alignment of its theoretical and experimental densities. IBSCZ is the most effective fluoride glass for radiation shielding

overall, according to metrics like mean free path, half-value layer, and mass and linear attenuation coefficients.

4. Conclusion

This work represents a major breakthrough in glass science by offering a novel theoretical method for assessing the density and radiation shielding properties of fluoride glasses. We were able to determine the packing density and theoretical density of fluoride glasses with remarkable accuracy by modifying the Makishima–Mackenzie model that is typically used for oxide glasses. These values closely matched the experimental values that were obtained using Archimedes' method. Our research enables anyone to refine the formula for improved precision. This validation creates a new path for predictive modeling in glass design in addition to filling the theoretical gap for fluoride systems. The novel IBSCZ glass ($40InF_3$–$15BaF_2$–$20SrF_2$–$5CdF_2$–$20ZnF_2$) was the most noteworthy of the fluoride glasses that were evaluated. Its fluorine-rich matrix and high-Z constituents, such as indium and cadmium, allowed IBSCZ to outperform traditional shielding materials like ilmenite and ordinary concrete in terms of gamma-ray attenuation over a broad energy spectrum (0.015–15 MeV). Its high shielding efficiency, lightweight design, and optical clarity are confirmed by the remarkably high MAC and LAC values along with low HVL, TVL, and MFP. IBSCZ glass is a next-generation material for high-performance, non-toxic, and compact radiation shielding in nuclear, aerospace, and medical applications because of these qualities. Overall, this work not only confirms the feasibility of theoretically modelling physical properties in fluoride glasses but also positions IBSCZ as a transformative material in radiation protection technologies.

Conflicts of Interest

The authors declare no conflict of interest.

Acknowledgments

The authors are thankful for the financial support extended by the Vision Group on Science and Technology (VGST), Government of Karnataka, under the scheme KSTEPS/VGST/ECRA/GRD No. 1251/2023-24.

AI Disclosure

The author(s) declare that no assistance is taken from generative AI to write this article.

References

Abd El-Moneim, A. (2019). Correlating bulk modulus and Poisson's ratio of alkali fluoride and oxyfluoride glasses with compositional parameters. *Journal of Fluorine Chemistry*, *221*, 48-55.

Abdel-karim, A.M., Fayad, A.M., El-Kashef, I.M., & Saleh, H.A. (2023). Influence of vanadium oxide on the optical and electrical properties of Li (oxide or fluoride) borate glasses. *Journal of Electronic Materials*, *52*(4), 2409-2420. https://doi.org/10.1007/s11664-022-10187-8.

Abouhaswa, A.S., & Taha, T.A.M. (2024). Synthesis, optical and magnetic properties of Nd2O3/borate strontium fluoride glasses. *Ceramics International*, *50*(7), 11032-11039. https://doi.org/10.1016/j.ceramint.2024.01.004.

Ahmmad, S.K., Jabeen, N., Ahmed, S.T.U., Hussainy, S.F., & Ahmed, B. (2021). Density of fluoride glasses through artificial intelligence techniques.*Ceramics International*, *47*(21), 30172-30177.

Almuqrin, A.H., Kumar, A., Prabhu, N.S., Jecong, J.F.M., Kamath, S.D., & Abu Al-Sayyed, M.I. (2022). Mechanical and gamma-ray shielding examinations of Bi2O3–PbO–CdO–B2O3 glass system. *Open Chemistry*, *20*(1), 808-815. https://doi.org/10.1515/chem-2021-0204.

Aloraini, D.A., Almuqrin, A.H., Sayyed, M.I., Al-Ghamdi, H., Kumar, A., & Elsafi, M. (2021). Experimental investigation of radiation shielding competence of Bi_2O_3-CaO-K_2O-Na_2O-P_2O_5 glass systems. *Materials*, *14*(17), 5061. https://doi.org/10.3390/ma14175061.

Alsaif, N.A., Shams, M.S., El-Refaey, A.M., Rammah, Y.S., Chaurasia, M.A., Siddiqui, N., & Ahmmad, S.K. (2023). On cobalt zinc boro sodium fluoride glasses doped with Y2O3: synthesis, artificial intelligence density prediction and dielectric spectroscopy. *Optik*, *281*, 170849. https://doi.org/10.1016/j.ijleo.2023.170849.

Bashter, I.I. (1997). Calculation of radiation attenuation coefficients for shielding concretes. *Annals of nuclear Energy*, *24*(17), 1389-1401. https://doi.org/10.1016/S0306-4549(97)00003-8.

Boolchand, P. (2000). *Insulating and semiconducting glasses* (Vol. 17). World scientific. Singapore.

Boutarfaia, A., & Poulain, M. (2002). Fluoride glasses in the InF_3–GaF_3–YF_3–PbF_2–CaF_2–ZnF_2 system. *Journal of Physics and Chemistry of Solids*, *63*(11), 2129-2133.

Brauer, D.S., Al-Noaman, A., Hill, R.G., & Doweidar, H. (2011). Density–structure correlations in fluoride-containing bioactive glasses. *Materials Chemistry and Physics*, *130*(1-2), 121-125.

Coşkun, A., Çetin, B., Yiğitoğlu, İ., & Canımkurbey, B. (2023). Theoretical and experimental investigation of gamma shielding properties of TiO_2 and PbO coated glasses. *International Journal of Computational and Experimental Science and Engineering*, *9*(4), 398-401.

Donald, I.W., Metcalfe, B.L., & Taylor, R.J. (1997). The immobilization of high level radioactive wastes using ceramics and glasses. *Journal of Materials Science*, *32*(22), 5851-5887.

Doremus, R.H. (1974). Mixed-alkali effect and interdiffusion of Na and K ions in glass. *Journal of the American Ceramic Society*, *57*(11), 478-480. https://doi.org/10.1111/j.1151-2916.1974.tb11395.x.

El-Desoky, M.M., Wally, N.K., Sheha, E., & Kamal, B.M. (2021). Impact of sodium oxide, sulfide, and fluoride-doped vanadium phosphate glasses on the thermoelectric power and electrical properties: structure analysis and conduction mechanism. *Journal of Materials Science: Materials in Electronics*, *32*(3), 3699-3712.

Feller, S. (2015). density, thermal properties, and the glass transition temperature of glasses. In Affatigato, M. (ed) *Modern glass characterization* (pp. 1-31). https://doi.org/10.1002/9781119051862.ch1.

Gayathri, T., Vijayakumar, M., Poojha, M.K., Muralidharan, G., Sankaran, K.J., & Marimuthu, K. (2024). Influence of Co-formers on the radiation shielding properties of zinc incorporated barium borate glasses for radioactive waste storage applications. *Optical Materials*, *153*, 115567. https://doi.org/10.1016/j.optmat.2024.115567.

Halimah, M.K., Hazlin, M.A., & Muhammad, F.D. (2018). Experimental and theoretical approach on the optical properties of zinc borotellurite glass doped with dysprosium oxide. *Spectrochimica Acta Part A: Molecular and Biomolecular Spectroscopy*, *195*, 128-135. https://doi.org/10.1016/j.saa.2017.12.054.

Inaba, S., & Fujino, S. (2010). Empirical equation for calculating the density of oxide glasses. *Journal of the American Ceramic Society*, *93*(1), 217-220. https://doi.org/10.1111/j.1551-2916.2009.03363.x.

Judith, N., & Oryema, B. (2024). A comparative study of photon radiation-shielding properties of different glass types for use in health facilities. *Reinvention: an International Journal of Undergraduate Research*, *17*(S1). https://reinventionjournal.org/article/view/1376.

Kawamoto, Y., Miyauchi, K., Shojiya, M., Sakida, S., & Kitamura, N. (2001). High-pressure densification of fluoride, GeS_2 and silicate glasses. *Journal of Non-Crystalline Solids*, *284*(1-3), 128-133.

Komatsu, T., Dimitrov, V., Tasheva, T., & Honma, T. (2021). Electronic polarizability in silicate glasses by comparison of experimental and theoretical optical basicities. *International Journal Of Applied Glass Science*, *12*(3), 424-442. https://doi.org/10.1111/ijag.16009.

Kumar, P., & Lenkennavar, S.K. (2025a). Analysis of radiation shielding and density prediction models for boro-tellurite glass systems, *13*(1), 53-70. https://doi.org/10.5772/intechopen.1008957.

Kumar, R.P., & Lenkennavar, S.K. (2025b). An investigation into empirical equations for predicting density and packing density parameters across diverse chemical compositions: a theoretical approach. *Prabha Materials Science Letters*, *4*(1), 66-77. https://doi.org/10.33889/PMSL.2025.4.1.006.

Kumar, S., Singh, K., & Kumar, D. (2024). B2O3 anomaly effect on crystallization and mechanical properties of soda-lime silicate glasses. *Materials Today Communications*, *39*, 109247.

Le Bourhis, E. (2014). *Glass: mechanics and technology*. John Wiley & Sons, Germany.

Macrelli, G., Varshneya, A.K., & Mauro, J.C. (2019). Simulation of glass network evolution during chemical strengthening: resolution of the subsurface compression maximum anomaly. *Journal of Non-Crystalline Solids*, *522*, 119457. https://doi.org/10.1016/j.jnoncrysol.2019.05.033.

Majewski, M.R., Woodward, R.I., Carreé, J.Y., Poulain, S., Poulain, M., & Jackson, S.D. (2018). Emission beyond 4 μm and mid-infrared lasing in a dysprosium-doped indium fluoride (InF3) fiber. *Optics Letters*, *43*(8), 1926-1929.

Makishima, A., & Mackenzie, J.D. (1973). Direct calculation of Young's moidulus of glass. *Journal of Non-Crystalline Solids*, *12*(1), 35-45. https://doi.org/10.1016/0022-3093(73)90053-7.

Mariyappan, M., Marimuthu, K., Sayyed, M.I., Dong, M.G., & Kara, U. (2018). Effect Bi_2O_3 on the physical, structural and radiation shielding properties of Er_3+ ions doped bismuth sodium fluoroborate glasses. *Journal of Non-Crystalline Solids*, *499*, 75-85. https://doi.org/10.1016/j.jnoncrysol.2018.07.006.

Mishra, N., Khan, U.A., Srivastava, A., & Asthana, N. (2024). Effect of the glass fiber orientation on mechanical performance of epoxy based composites. *Prabha Materials Science Letters*, *3*(2), 175-190. https://doi.org/10.33889/PMSL.2024.3.2.011.

Musgraves, J.D., Richardson, K., & Jain, H. (2011). Laser-induced structural modification, its mechanisms, and applications in glassy optical materials. *Optical Materials Express*, *1*(5), 921-935.

Nazabal, V., Poulain, M., Olivier, M., Pirasteh, P., Camy, P., Doualan, J.L., Guy, S., Djouama, T., Boutarfaia, A., & Adam, J.L. (2012). Fluoride and oxyfluoride glasses for optical applications. *Journal of Fluorine Chemistry*, *134*, 18-23. https://doi.org/10.1016/j.jfluchem.2011.06.035.

Ornketphon, O., Kaewjaeng, S., Meejitpaisan, P., Mutuwong, C., Chaipaksa, W., Sommat, V., & Kaewkhao, J. (2024). Photon shielding properties of oxyfluoride aluminophosphate glass added with Sb_2O_3 by using PHITS Monte Carlo simulation and experimental methods. *Radiation Physics and Chemistry*, *224*, 111993.

Panda, S., & Prabha (2022). Biomolecular piezoelectric materials for biosensors. *Materials Science Letters*, *1*(1), 37-49. https://doi.org/10.33889/PMSL.2022.1.1.006.

Poulain, M., Soufiane, A., Messaddeg, Younes, Aegerter, Michel, A. (1992). Fluoride glasses: synthesis and properties. *Brazilian Journal of Physics, 22*, 205-217. http://dx.doi.org/10.22028/D291-24118.

Priven, A.I., Mazurin, O.V. (2003). Comparison of methods used for the calculation of density, refractive index, and thermal expansion of oxide glasses. *Glass Technology*, *44*(4), 156-166.

Putra, O.A., Faniandari, S., & Yutomo, E.B. (2025). Investigation of TeO_2-based Boro tellurite glass as a radiation shield: Effects of composition on attenuation parameters. *International Journal of Research and Review, 12*(3), 1-7. https://doi.org/10.52403/ijrr.20250351.

Scholze, H. (1991). *Glass—nature, structure and properties*. Springer-Verlag, New York. ISBN 0-387-97396-6.

Sekaran, S.A.R., Vijayakumar, M., Suriyamurthy, N., Alqahtani, M.S., & Marimuthu, K. (2024). Investigations of substantial effect on physical, structural, optical and radiation shielding properties of nitrates integrated alkaline oxyfluoro phospho-silicate glasses. *Progress in Nuclear Energy, 175,* 105330.

Shannon, R.D. (1976). Revised effective ionic radii and systematic studies of interatomic distances in halides and chalcogenides. *Foundations of Crystallography*, *32*(5), 751-767.

Shannon, R.T., & Prewitt, C.T. (1969). Effective ionic radii in oxides and fluorides. *Structural Science*, *25*(5), 925-946.

Shannon, R.T., & Prewitt, C.T. (1970). Revised values of effective ionic radii. *Structural Science*, *26*(7), 1046-1048.

Shaukat, S.F., Dong, Y.M., Farooq, R., & Hobson, P.R. (2001). Relationship between composition, density and refractive index for heavy metal fluoride glasses. *Journal of Shanghai University (English Edition)*, *5*(3), 201-204.

Shelby, J.E. (2005). *Introduction to glass science & technology*. The Royal Society of Chemistry. Cambridge, USA.

Shi, Y., Tandia, A., Deng, B., Elliott, S.R., & Bauchy, M. (2020). Revisiting the Makishima–Mackenzie model for predicting the young's modulus of oxide glasses. *Acta Materialia*, *195*, 252-262.

Slater, D.P., & Fong, B.S. (1982). Density, refractive index, and dispersion in the examination of glass: their relative worth as proof. *Journal of Forensic Sciences*, *27*(3), 474-483. https://doi.org/10.1520/JFS12159J.

Stroganova, E.E., Mikhailenko, N.Y., & Moroz, O.A. (2003). Glass-based biomaterials: present and future (a review). *Glass and Ceramics*, *60*(9), 315-319.

Tanabe, S., Takahara, K., Takahashi, M., & Kawamoto, Y. (1995). Spectroscopic studies of radiative transitions and upconversion characteristics of Er3+ ions in simple pseudoternary fluoride glasses MF n–BaF_2–YF_3 (M: Zr, Hf, Al, Sc, Ga, In, or Zn). *Journal of the Optical Society of America B*, *12*(5), 786-793.

Tian, J., Zhao, Y., Huang, Y., Li, Y., Zhang, C., Peng, S., & Liu, Y. (2024). Theoretical prediction of Vickers hardness for oxide glasses: Machine learning model, interpretability analysis, and experimental validation. *Materialia*, *33*, 102006. https://doi.org/10.1016/j.mtla.2024.102006.